Microtubule-induced nuclear envelope fluctuations control chromatin dynamics in Drosophila embryos

Bernhard Hampoelz, Yannick Azou-Gros, Roxane Fabre, Olga Markova, Pierre-Henri Puech, Thomas Lecuit

▶ **To cite this version:**

HAL Id: inserm-01117494

https://inserm.hal.science/inserm-01117494

Submitted on 17 Feb 2015

Microtubule induced nuclear envelope fluctuations control chromatin dynamics in Drosophila embryos

Bernhard Hampoelz, Yannick Azou, Roxane Fabre*, Olga Markova Pierre-Henri Puech* and Thomas Lecuit

IBDML, UMR6216 CNRS-Université de la Méditerranée. Campus de Luminy, case 907. 13288 Marseille Cedex 09. France.
* INSERM UMR 600 / CNRS UMR 6212, Case 937 - 163, avenue de Luminy, 13288 Marseille Cedex 09 - France

Summary

Nuclear shape is different in stem cells and differentiated cells and reflects important changes in the mechanics of the nuclear envelope (NE). The current framework emphasizes the key role of the nuclear lamina in nuclear mechanics and its alterations in disease [1, 2]. Whether active stress controls nuclear deformations and how this stress interplays with properties of the NE to control NE dynamics is unclear. We address this in the early *Drosophila* embryo, where profound changes in NE shape parallel the transcriptional activation of the zygotic genome. We show that microtubule (MT) polymerization events produce the elementary forces necessary for NE dynamics. Moreover, large-scale NE-deformations associated with groove formation require concentration of microtubule polymerization in bundles organized by Dynein. However, MT bundles cannot produce grooves when the farnesylated inner nuclear membrane protein Charleston/Kugelkern (Char/Kuk) is absent [3, 4]. Although it increases stiffness of the NE, Char/Kuk also stabilizes NE deformations emerging from the collective effect of MT polymerization forces concentrated in bundles. Finally we report that MT induced NE deformations control the dynamics of the chromatin and its organization at steady state. Thus, the NE is a dynamic organelle, whose fluctuations increase chromatin dynamics. We propose that such mechanical regulation of chromatin dynamics by MT may be important for gene regulation.

Introduction

Nuclei contain and protect the genetic material of eukaryotic cells. Although nuclei are often spherical, nuclear shape can change significantly between cell types and during cell differentiation or aging (only refs).

As the organelle's limiting compartment, the nuclear envelope (NE) is a key determinant of nuclear morphology. The nuclear lamina, a meshwork underlying the inner nuclear membrane in metazoa, is crucial for the structural integrity of nuclei [5]. Lamins, the major constituents of the lamina, not only support the structure of nuclei but also play important roles in transcription, replication or chromatin organization [6]. In most species there are two different types of lamins: a ubiquitously expressed membrane anchored B-type Lamin, and one or more A-type Lamins, which become only expressed when cells start to differentiate and localize to the NE and the nucleoplasm. A-type Lamins control the mechanics of the NE, and are responsible for the increased stiffness of nuclei in differentiated cells compared to stem cells[7]. Thus, nuclear mechanics must be tightly regulated. Changes in nuclear mechanics are accompanied by defects in gene expression and a distorted nuclear morphology [1, 2, 8]. It is thus essential to decipher the mechanisms regulating nuclear mechanics and morphogenesis. By analogy to cell shape changes controlled by generators of forces and the mechanical response of the cortex, we sought to investigate the origins of nuclear deformations and to delineate active forces that shape nuclei and the mechanical properties of the NE.

We address this in the physiological context of the early *Drosophila* embryo, where profound changes in nuclear shape parallel transcriptional activation of the zygote. After 13 rounds of mitosis without cytokinesis, about 6000 somatic nuclei at the embryo periphery are packaged by the invaginating plasma membrane (PM) during interphase 14, a process called cellularisation[9]. Nuclei are regular and spherical when cellularisation starts, but subsequently elongate into ellipsoids and acquire an irregular, lobulated morphology[3, 4](Fig. 1a,b). While nuclear elongation depends on microtubules (MTs) [10], it is largely unclear how the NE becomes lobulated. Yet it does not involve A-type Lamin, which is expressed only later in development [11]. Instead, the farnesylated inner NE protein Charleston/Kugelkern (Char/Kuk), which is strongly up-regulated at the onset of cellularisation, is required for NE-morphogenesis[3, 4]. Similar to membrane anchored Lamins, ectopic expression of Char/Kuk exacerbates NE lobulation in flies [12] but also other systems [13] How Char/Kuk regulates NE morphogenesis is not understood.

Nuclear morphogenesis occurs concomitantly with the up-regulation of the zygotic genome. In animals, this key developmental switch involves a massive up-regulation of transcription as well as major re-arrangements in chromatin structure and marks the onset of differentiation[14]. In *char/kuk* mutants, transcription of certain zygotic genes is changed [3]. This suggests that nuclear morphology contributes to gene expression.

Here we investigate the mechanisms of NE morphogenesis by focusing on the dynamics of the NE. Such dynamics is expected to reflect the presence of force generators. We show that nuclear deformation during *Drosophila* cellularisation results from a combination of active cytoplasmic stresses and developmentally controlled mechanical properties of the NE. While microtubule polymerization provides the elementary force necessary for NE dynamics, large-scale deformations of the NE into grooves require sustained MT polymerization within bundles organized by the cytoplasmic motor Dynein. However, to fully deform, nuclei need the farnesylated inner NE protein Char/Kuk, which controls NE stiffening during cellularisation. Finally we show that the dynamics of the NE during cellularisation promotes chromatin mobility and steady-state organization during zygotic induction.

Results

Microtubules control NE morphogenesis during *Drosophila* cellularisation

We focused our analysis on the dynamics of NE morphogenesis during early *Drosophila* development..For live analysis the NE was labeled with fluorescent Wheat Germ Agglutinin (WGA), a lectin, which within the NE binds to a component of the Nuclear Pore Complex (NPC) [15]. Since NPC disassemble during mitosis, entry into interphase could be precisely timed by the re-appearance of WGA at the nuclear rim. Our time-lapse analysis revealed that starting with Interphase 14 the NE remodels in a highly dynamic fashion (Supp Movie 1). NE- dynamics was not restricted to cellularisation but was also present in nuclei from gastrulating embryos or from wing discs isolated from third instar larvae (data not shown). We deciphered three phases in NE morphogenesis during cellularisation: 12-15 min after mitosis, the NE lost its round shape and formed polygons, which later progressively acquired grooves during lobulation (Supp Movie S1, Fig. 1a,b-b"). The dynamics of groove formation was apparent in kymographs in the form of NE-lateral deformations (Fig. 1h,h'), which increased in amplitude over time as grooves formed (p=7.23 x10^{-5}) (Fig. 1j). The formation of grooves could be a passive consequence of persistent growth of the NE during cellularisation. However, two observations do not support this view. First, measurements of the NE surface increase by 3D reconstruction from serial z-sections showed that 87% of surface increase preceded groove formation (Fig. S1 a). Thus groove formation did not correlate in time with total NE surface increase. Second, kymographs showed that grooves could be reversible within a few minutes, suggesting that active mechanisms might underlie their formation (Supp movie 1, Fig. 1h"). We next tested whether NE lobulations form in response to active stress exerted by the invaginating membrane and contractile furrow canals as they pass around nuclei. We imaged the NE in *slam* RNAi embryos where plasma membrane invagination is strongly delayed up until the end of nuclear elongation [16]. In these embryos, groove formation was indistinguishable from wild type controls (Fig. S1b,b').

This led us to hypothesize that groove formation is an active process operating locally and specifically at the NE as already suggested in cell culture [17]. During cellularisation, MTs form a tight basket around nuclei. They are organized from a pair of centrosomes, which is apically attached to nuclei (Fig 1d), and are known to be required for nuclear elongation [9]. We investigated the relationship between MT distribution and NE grooves. We imaged embryos expressing tubulin::GFP (Supp Movie 2, Fig. 1e) and measured a gradual concentration of tub::GFP at the NE at the expense of the cytoplasm during cellularisation (Fig. 1f). Similar observations were made with endogenous alpha-Tubulin labeled with an antibody (Fig. 1g). Remarkably, MTs consistently decorated grooves (Supp Movie 2 and Fig. 1e). To test whether MTs could control groove formation we injected the MT de-polymerizing drug Colcemid during early cellularisation. As previously reported, elongation of nuclei was blocked [10] but NE surface continued to grow, although reduced (Fig. S2a). Kymographs indicated that the dynamics of the NE was drastically impaired compared to wild type (p=1.34 x10^{-4}) (Supp Movie 3, Fig. 1c-c",i,i',j) and reversible grooves never formed. However, live imaging revealed the existence of irreversible buckling of the NE at late stages, specifically when NE growth brings nuclei into contact. In this case, deformations form passively in response to the compressive stress imposed by NE growth (Supp Movie 3, Fig. 1c-c"). We conclude that MTs are concentrated in grooves and essential for NE remodelling.

Dynamic microtubules are organized in stationary bundles at the NE

This suggests that MTs might constrain the NE and deform it locally like static posts. Consistent with this, kymograph analysis from embryos expressing tub::GFP indicated that MTs were organized within stationary bundles that kept their lateral localization along the NE (Fig. 2a,b). Bundles were present during early (Fig. 2a,a') and late cellularisation (Fig. 2b,b'). Acetylated and thus relatively stable MTs have been reported to localize at the NE during cellularisation but not in earlier interphases [18]. This acetylated pool represented a subset of the overall MT network around nuclei (Fig. 2c). Most grooves (79.8 +/-0.09 %, n=190) were occupied by acetylated MTs. Nonetheless, MT bundles were also found outside grooves since half of the NE lobules (49.8 +/-0.1%, n=407) contained acetylated MT spots (Fig. 2d,e). Together, this supports the view that MT bundles behave like stable posts constraining the NE. To further test this we probed MT dynamics by performing FRAP experiments in embryos expressing tub::GFP. Strikingly however, MTs within bundles appeared unexpectedly dynamic (recovery fraction= 64+/-21%, $t_{1/2}$ =6.8+/-5.1 seconds) (Fig. 2f,g). Tub::GFP recovered at the same position along the NE where the bundle was located before bleaching and we did not observe lateral redistribution of MTs from adjacent regions of the NE (Fig 2f,f',f"). This indicates that MTs are inherently dynamic within apically-basal oriented stationary bundles and do not slide laterally along the NE. MTs were equally dynamic before and after nuclei lost their regular structure (p=0.275) and, in late cellularizing embryos, grew similarly in grooves and lobules (p=0.354) (Fig.2g). Imaging a GFP-fusion of the MT plus end tracking protein EB1 confirmed the dynamic nature of the MT network along the NE (Fig.3c).

NE fluctuations require dynamic microtubules

These observations led us to consider another model where MT polymerization might play an active role in NE deformations and groove formation. Closer examination of NE dynamics revealed the existence of two modes of fluctuations that could be deciphered from kymographs: apart from the large (1.7 +/-0.2 μm) and few minutes long deformations associated with grooves (Fig. 1h',i, Fig 3a), the NE showed 'high frequency' fluctuations with a lower amplitude of up to 300 nm (Fig.3a'). Interestingly, MT de-polymerization caused a significant reduction of the latter fluctuations (p=6.25x10^{-28}), indicating that those likely result from impulsions associated with MT polymerization events (Fig.3b). Consistent with this, NE fluctuations were also low in interphase 13 embryos ((Fig 3b, p=3.73 x10^{-14} compared to IP14), at a stage when MT are not concentrated at the NE. To test this further we injected the MT stabilizing drug Taxol. This decreased (albeit did not abolish) MT dynamics, since EB1::GFP was reduced at the NE (Fig.3c,c') and Microtubules recovered less and more slowly (recovery fraction= 46+/-16%, $t_{1/2}$= 22.0 +/-6.8 seconds) compared to wild type after photobleaching (Fig. 3d). Taxol injection significantly reduced the high frequency fluctuations of the NE (p=1.66x10^{-7}) (Fig.3e). Taxol prevents incorporation of tubulin monomers, but also inhibits de-polymerization of existing tubules. Consequently, the lifetime of MT bundles at the NE was increased following Taxol injection (Fig. 3f,f',g) (p=0.0013) while the number of bundles was similar to controls (p=0.319). In this case, MT bundles became more stable than in controls. However, the NE was more regular and formation of grooves was strongly impaired after Taxol injection (Fig. 3h-j). We conclude that the NE is a very dynamic organelle exhibiting two modes of fluctuations that are both dependent on MT dynamics. Moreover, grooves emerge from the collective effects of MT polymerization events concentrated in stationary (but not stable) bundles at the NE.

Cytoplasmic Dynein bundles Microtubules at the NE

This model predicts that affecting MT bundling should also affect NE lobulation. Dynein may affect MT concentration at the NE, e.g. by regulating bundle organization. Dynein connects MTs to cargo molecules or organelles and regulates centrosome attachment at the NE in *C.elegans* [19] and *Drosophila* [20]. During mammalian prophase NE-attached Dynein facilitates envelope breakdown by MT-induced NE tearing [21, 22]. To specifically interfere with Dynein activity during cellularisation we injected anti-Dynein heavy chain (Dhc) or anti-Dynein intermediate chain (Dic) neutralizing antibodies into embryos after they entered Interphase 14. This led to decreased elongation of nuclei, resembling a weak colcemid phenotype. (Fig. S2b). To check MT integrity in embryos with reduced Dynein activity we co-injected neutralizing antibodies and WGA-Alexa 555 into cellularising embryos expressing tub::GFP and compared tub::GFP levels at the NE within the same embryos in-and outside the injection area (Fig. 4a-c). Ratios between NE-decorating and cytoplasmic tub::GFP were significantly reduced in regions where the neutralizing anti-Dynein antibodies had been injected, compared to adjacent regions (Fig. 4c). Similar effects were observed for anti-Dhc (n=20 nuclei, p=1.28 x 10^{-7}) and anti-Dic antibodies (n=50 nuclei, p=2.29 x 10^{-8}) but not with anti-GST antibodies, where ratios were approximately equal in- and outside the injected region (n=50 nuclei, p=0.79) (Fig. 4c). To test if this is due to reduced MT polymerization [23], we quantified EB1::GFP levels at the NE and found no significant difference between anti-Dhc antibody-targeted or untargeted areas within the same embryos (Fig. 4d, e). Consequently MT-polymerization dependant fluctuations of the NE were similar in wild type embryos or after Dynein inhibition (p=0.563) (Fig.4f). Instead, tub::GFP kymographs showed that bundles were shorter lived and splayed out following anti-Dhc antibody injection in contrast to control regions where bundles were persistent (p=5.65 x 10^{-34}) (Fig. 4g-g'' h). We conclude that Dynein is required for MT bundle integrity at the NE. Remarkably, in contrast to a control anti-GST antibody, injection with either anti-Dhc or anti-Dic antibodies reduced significantly the formation of grooves (Fig. 4i-l). Together this suggests that while MT dynamics is responsible for high frequency fluctuations of the NE, bundling of dynamic MTs is a key determinant of large-scale NE deformations into grooves through the collective effect of polymerization forces. Dynein could also control NE deformations in grooves by coupling to the NE directly and using MT bundles as a (dynamic) scaffold.

The farnesylated protein Char/Kuk mediates MT induced nuclear deformations

How do these forces interplay with the material properties of the NE to yield effective deformations? The farnesylated inner NE-protein Char/Kuk, is essential for NE lobulation during cellularisation (Fig 5a-a'')[3, 4]. We further studied the function of Char/Kuk in light of our findings that the NE is a dynamic structure which fluctuates in response to dynamic MTs. In *char/kuk* mutants the NE displayed high frequency oscillations similar to wild type (Fig S3c) but eventually fails to deform into grooves (Supp Movie 4). Consistent with this, neither MT attachment (ref Pilot et al 2006) at the NE nor MT dynamics or organization into bundles were changed in cellularising *char/kuk* embryos (Fig S3a,b). Considering its localization at the inner nuclear membrane, this argues that Char/Kuk affects nuclear deformations by exclusively modulating NE material properties, and that these properties may be essential for NE deformations.
The visco-elastic properties of the NE could indeed control its deformability. We tested this with Atomic Force Microscopy (AFM), which has been successfully used to probe the mechanical characteristics of cells but also of isolated nuclei [24]. The application of a given force by the AFM cantilever tip indents the nuclei. From the

resulting pressing curve the material's stiffness expressed by the Young modulus E can be obtained with a suitable model corresponding to the experimental situation (Fig 5e, e'). We first probed immobilized nuclei that were isolated from wild type embryos either before Interphase 14 (blastoderm stage, n=15 nuclei) or during Interphase 14 (n=20 nuclei) and obtained Young moduli in a similar range than published for other systems [1]. Interestingly, "younger" nuclei appeared soft with E moduli far below the values measured for nuclei from Interphase 14 embryos (p=4.74 x 10^{-8}) (Fig. 5f), indicating that stiffness rises as grooves form. Strikingly, nuclei from *char/kuk* mutant Interphase 14 embryos (n=46 nuclei) showed much lower E moduli than same-age wild type nuclei (p=5.07 x 10^{-9} for the comparison of *char/kuk* with Interphase 14 wild type embryos) (Fig. 5f). We conclude that Char/Kuk induces stiffness of the NE during cellularisation.

However, several lines of evidence indicate that Char/Kuk controls additional properties of the NE under stress. Over-expression of *char/kuk* increases NE deformations during cellularisation and induces them earlier (ref)(Fig 5b-b''). Importantly this depends on the presence of MTs, in agreement with our model that sustained dynamic MTs impose the active stress required for NE morphogenesis (Fig.5i-i''). However, nuclei from *char/kuk* over-expressing embryos were not stiffer than nuclei with wild type levels *(p=0.491)(Fig 5f)*. Second, nuclei from embryos with elevated levels of Dm0 showed a significantly increased stiffness prior to Interphase 14 compared to nuclei from control embryos (p=4.95 x 10^{-5})(Fig 5f), but did not deform the NE as strong as in 6x *char/kuk* embryos during cellularisation (Fig 5c-c''). Finally, increased levels of Dm0 cannot rescue *char/kuk* mutants (Fig 5d-d'')[13]. Overall this argues against a model, where Char/Kuk regulates deformation of the NE by solely increasing its stiffness.

We thus tested whether *Char/Kuk* could modulate nuclear viscosity. We assessed this by comparing the mode of force dissipation after pressing on isolated nuclei with the AFM cantilever. However, recording force curves over 10 seconds did not reveal significant differences between wild type nuclei from embryos before and during cellularisation or between the latter and nuclei isolated from *char/kuk* embryos in IP 14 (Fig 5g).

This led us to propose that Char/kuk could act structurally to stabilize NE deformations, which were initially induced by progressive and bundled MT stress. Once stabilized the NE could then stay deformed without any further need of a cytoplasmic force. To test this we de-polymerized MTs later in cellularisation, once nuclei have lost their round shape. However, at this stage the invaginated plasma membrane restricts MT de-polymerization basally to the cellularisation front (Fig 5h). To overcome this we de-polymerized MTs in embryos over-expressing char/kuk, which acquire NE deformations earlier in cellularisation compared to wild type embryos (Fig 5b-b''). While the application of Colcemid in early IP14 prevents any NE deformation and resembles similarly treated embryos with wild type levels of char/kuk (Fig 5i-i''), later MT de-polymerization conserved grooves that had already been formed (Fig 5j-k'')). Importantly, in such conditions NE grooves can further deepen, indicating buckling of the pre-stressed NE (Fig 5k-k''). This proposes a two-tiered mechanism for NE deformation during Drosophila cellularisation. Sustained MT polymerization forces in bundles first nucleate deformations of the NE. Subsequently these deformations are enhanced into grooves by the activity of Char/Kuk at the INM, which causes NE stiffening and buckling in response to stress.

NE dynamics induces chromatin mobility

We finally addressed the functional significance of NE fluctuations and lobulation induced by MTs. We tested whether NE dynamics and deformation could be transmitted to the nucleoplasm and thereby globally 'agitate' the chromatin. This

could contribute to the progressive activation of the chromatin and to zygotic activation occurring during cellularisation [4, 14].

We imaged a subset of the chromatin labeled by a GFP fusion of the Histone variant H2Av during cellularisation[25]. H2Av::GFP localized throughout nuclei and was enriched in spots, which were very dynamic (Fig 6a,a', Supp Movie 5). Spot dynamics was not restricted to the nuclear periphery but occurred also inside the nucleoplasm. These central H2Av::GFP spots occasionally followed NE movements (Fig 6a'). We measured mean velocities of H2Av::GFP by applying particle image velocimetry (PIV) to quantitate flow fields in the nucleoplasm. (Fig 6b,c,c'). The mean velocity was commensurate with that of the NE (compare the mean speads) and increased from interphase 13 to interphase 14, concomitant with the progressive recruitment of dynamic MTs at the NE and the emergence of NE fluctuations (Fig 6c). Strikingly, H2Av::GFP mean velocities were significantly smaller in colcemid injected embryos at interphase 14 compared to controls (Fig. 6d). Similar results were obtained when the PIV analysis was done considering only the most central region of the nucleoplasm at a distance from the NE (Fig 6c') thereby reflecting global effects on the chromatin. In *char/kuk* mutant embryos, H2Av::GFP flow mean velocities were also significantly reduced, albeit not to the same extent than in colcemid treated embryos. Given that in *char/kuk* mutants, the high frequency fluctuations of the NE are normal while lobulations do not form, this suggests that H2Av::GFP dynamics is induced by both small and large scale deformations.

Since PIV measures apparent flow patterns and does not follow individual chromatin spots, we tracked bright H2Av::GFP spots that could be resolved in kymographs in middle sections through the nucleoplasm (Fig 6d-g). In a given confocal plane, the length of an H2Av::GFP trace in the nucleoplasm measures the persistence of H2Av::GFP spots in this plane. Although we cannot fully rule out cases of spontaneous assembly or disassembly of spots, kymograph analysis of different z planes indicate that H2Av::GFP spots indeed moved along the apical basal axis (Fig S4). H2Av::GFP spots were less mobile when NE dynamics was reduced (eg. colcemid treated, Fig 6f) or groove formation was inhibited (*char/kuk* mutants, Fig 6g) as indicated by the less ragged traces in kymographs..Accordingly, the corresponding persistence times (length of kymograph traces) of chromatin spots were reduced compared to wild type embryos during cellularisation (Fig 6h,h').

A portion of heterochromatin restricts apically into centromeric chromocenters during *Drosophila* cellularisation but not before[14] (Fig S4a-b''). Chromatin movement due to NE dynamics could therefore contribute to the establishment of chromatin organization. Indeed HP-1 labeled heterochromatin fails to concentrate apically and overlaps with euchromatin upon MT de-polymerization (Fig S4c-c''). A similar phenotype was seen in *char/kuk* embryos: In contrast to a previous report we detected HP-1 labelled chromatin (ref), but the separation between hetero and euchromatin was less pronounced (Fig S4d-e''). Nuclei in cellularising *char/kuk* mutants initially elongate normally, before they round up and loose contact with the apical cortex[4] (Fig S4d,e). Our observation that chromatin domains separation is disrupted within the elongation phase argues that mixing of hetero- and euchromatin is not a mere consequence of reduced nuclear length (Fig S4d-d'').

Discussion

In summary, our results indicate that nuclear shape in *Drosophila* embryos is not simply determined by nuclear factors that control deformability. Instead we show that NE dynamics and morphogenesis requires the interplay between active stresses exerted by polymerization of MTs organized in bundles and properties of the NE.

Surprisingly, MTs do not shape the NE like a static scaffold that constrains inherent dynamics of the NE. Rather, we find that MT dynamics is essential. Polymerization of MTs produces high frequency, small fluctuations but is not capable of large-scale deformations into grooves. Groove formation requires MT polymerization within bundles, a property which we show depends on Dynein. We thus propose that pushing forces emanating from MT polymerization events are the fundamental active process that underlies nuclear deformations. However their organization in bundles is essential for lobulation. Bundling of growing MTs along a stationary core most likely increases their ability to produce force. In vitro experiments and simulations showed that MTs in a bundle reach pushing forces much higher than the stall force of individual MTs [26]. Moreover, relaxation of grooves may be facilitated with bundles, since pushing of a bundle against obstacles was shown to induce collective catastrophe [26]. Bundle integrity is ensured by cytoplasmic Dynein. Although we did not detect an enrichment of Dynein at the NE in antibody-stainings (data not shown), Dynein could be localized at the NE, where it would allow bundle cohesion and attachment. In *Drosophila* photoreceptors as well as *C. elegans* embryos and gonads, Dynein is recruited to the NE by KASH (*K*larsicht-*A*nc1 *S*yne-1 *H*omology) domain proteins [27, 28 29]. KASH proteins are part of the conserved LINC (linker of the nucleoskeleton and cytoskeleton) complex, which spans the NE. LINC proteins have a conserved role in positioning and anchoring nuclei and whether they could also regulate nuclear morphology will be important to test [30].

Interestingly, LINC proteins are also used to move chromosome loci by mediating forces generated by cytoskeletal elements[31]. During meiosis, telomeres in yeast or pairing centers in *C.elegans* interact with LINC proteins at the INM. Pairing of homologous regions occurs via force generation at the cytoskeleton and transmission of this force to the INM. Likewise in fission yeast LINC proteins together with the INM protein Ima1 connect the spindle pole body (SBP) with centromeric heterochromatin during interphase[32]. In contrast to the targeting of specific chromosome loci as telomeres or centromeric heterochromatin, the global movement of H2Av::GFP labeled chromatin during *Drosophila* cellularisation is likely to be a very general feature of the nucleoplasm and thus would not require specific attachments of selected genomic regions to the NE. After they mediate clustering of telomeres at the NE adjacent to the SBP, the yeast LINC proteins ensure that telomeres keep this position throughout meiotic prophase. During this period MTs attached to the SBP drag the whole nucleus back and forth in a Dynein dependant manner[33]. It was suggested that this rocking facilitates chromosome pairing and on the contrary agitates the nucleus sufficiently to disassemble non-homologous interactions. By analogy, MT induced oscillations of the NE could serve as a means to generally enhance chromatin mobility at the onset of zygotic transcription. The recently established concept of transcription factories, where active loci are pulled into pre-assembled clusters of polymerase and transcription factors as sites of mRNA production demands a mobile chromatin[34]. The enhanced 'diffusion' of chromatin spots in the nucleoplasm could also increase the probability of interactions with another locus on the same or another chromosome, and tune cis-regulatory interactions[35]. Interactions with the NE could also be more frequent. It will be important to investigate whether the dynamics of the chromatin in the nucleoplasm tunes the probability of chromatin/chromatin and chromatin/NE interactions and whether gene regulation may be limited by the apparent 'diffusion' of the chromatin. Interestingly transcription is affected in char/kuk mutants. Whether MT induced chromatin diffusion participate in large scale gene regulation will be interesting to test.

Although necessary, MT polymerization forces are not sufficient to produce grooves in the NE. These deformations require specific material or structural properties of the

NE. Our work sheds new light on this process. Comparison of human embryonic stem cells and differentiated cells indicates that deformability is usually increased when stiffness is reduced (and vice versa), for instance due to absence or knock-down of A-type Lamins [736]. Lamin C, the *Drosophila* A-type lamin is not expressed during cellularisation, and nuclear deformability is instead controlled by the farnesylated inner nuclear membrane protein Char/Kuk. Char/Kuk increases the stiffness of the NE, and it is required for large deformations most likely because stiffness is required for the pre-stressed NE to buckle. However, Char/Kuk likely controls other properties of the NE since it cannot be rescued by elevated levels of Dm0 which also increases stiffness. Likewise, overexpressed Dm0 does not enhance lobulation. Char/Kuk could stabilize transient and small deformations imposed by microtubules. Stabilization of NE curvature would work as a ratchet and allows the temporal integration of small polymerization forces contributed by individual MTs in bundles. Progressive enrichment of char/kuk at the INM during Interphase 14 could explain why grooves only form starting with mid-cellularisation, despite the presence of a MT network capable to deform the NE already earlier. The need for a critical threshold of Char/Kuk at the INM to allow deformation would also explain the precocious appearance of grooves in embryos that over-express char/kuk. The relative amounts of MT polymerization forces and NE stiffness would define the threshold above which buckling is possible,. Ectopic expression of the farnesylated INM proteins Char/Kuk and Dm0 is sufficient to deform nuclei and induces chromatin modifications reminiscent of Lamin mutations that give rise to Laminopathies as the premature aging disease Hutchinson Gilford Progeria Syndrom (HPGS)[12]. This disease is caused by mutations in a splice site of a human A-type Lamin that renders the produced protein constitutively membrane bound[37]. Whether membrane ruffling as seen in cells from HPGS patients and NE lobulation in *Drosophila* embryos are analogous will be interesting to address.

The *Drosophila* embryo is a powerful physiological system in which the mechanics of NE deformation can be studied in detail and in its endogenous developmental context. NE dynamics and deformations induce chromatin diffusion and are concomitant with zygotic induction, which marks the onset of differentiation in animals. Unraveling the complex machineries that control NE and chromatin dynamics is an important step to understand how these could contribute to the transition from pluripotency to differentiation in *Drosophila*.

.

Material and Methods

Fly strains and antibodies

The following fly lines were used: yw; UAS-*EB1::GFP, mattubGAL4VP16/ CyO* [38], *yw sqh[AX3];sqh-Sqh::GFP* (gift of R. Karess) , H2Av::GFP (gift of G. Cavalli)
tub::GFP (full genotype: *w^1118^; P{GAL4::VP16-nos,UTR}CG6325^MVD1^,P{UASp-GFPS65C-aTub84B}3*) (BL-7553), UAS::Dm0, *kuk* [3], 6xkuk. *yw* flies were used as wild type controls
Antibodies: mouse anti-α Tubulin (1:500, Sigma), mouse anti-Acetyl Tubulin (1:500, Abcam), rabbit anti-H3K4diMe (1:500, Upstate), mouse anti-HP1 (1:50, DSHB). For Immunofluorescence experiments, embryos were dechorionated, washed and fixed in 4% PFA and devitellinized by Methanol popping. For anti-αTubulin stainings, embryos were fixed for 1 min in 37% PFA.
Injections were performed with Colcemid (1.25 mM, Sigma), Taxol (Paclitaxel, 20 mg/ml, Sigma), WGA-Alexa488 or WGA-Alexa555 (100 µg/ml, Molecular Probes) and the following antibodies: mouse anti-Dhc [39], mouse anti-Dic (300 µg/ml, Millipore), mouse anti-GST (300 µg/ml, Eurogentec). dsRNAi probes for *char/kuk* and *slam* were injected at 5 µM.

Embryo injections and Live Imaging

Staged blastoderm embryos were treated as described [40] and injected with fluorescently labeled WGA. WGA dis- and re-appearance during and after mitosis 13 was used to time the onset of cellularisation. Drugs or neutralizing antibodies were injected shortly after embryos entered Interphase 14 and embryos were filmed using a 100x /1.3 oil objective on a Zeiss LSM 510 confocal microscope. 3D reconstruction of nuclei was done from 0.5 µm distant z-sections using the 3D segmentation editor of Amira. Nuclear surfaces were calculated with the 3D Virtual Embryo software [41].

Quantifications and statistics

Quantification of NE-dynamics: Staged embryos injected with fluorescently labeled WGA were recorded at a confocal microscope in top views. To measure large scale NE-deformations nuclei were imaged in one z-plane at 50% of nuclear height for 6 min with a frame taken every 5 seconds. 2.5 μm wide Kymographs spanning the WGA-signal (Fig.1h,h') were created with the Metamorph software after correcting each selected nucleus for drift using stack cross-correlation in EMBL ImageJ. Groove associated NE deformations were measured on kymographs as distance in µm between the most lateral positions of the WGA signal within the 6 min interval (Fig.1g',3a).
To measure high frequency fluctuations of the NE, WGA intensity was measured after correcting for drift as described above along lines spanning the NE every 5 seconds over 6 min using Metamorph. Pixel-positions of the maximal WGA intensity along the length of the linescan for each frame were detected in Matlab. Standard deviations of those positions within 1 min intervals were calculated, giving an approximation for the fluctuation of the NE on a short time scale (Fig. 3a').
Intensity measures of tub::GFP: Tub::GFP expressing cellularising embryos injected with fluorescently labeled WGA were recorded at distinct time-points throughout cellularisation at a confocal microscope in top views. Start of interphase14 was timed by re-appearance of WGA at the NE and disappearance of spindles. Confocal z-sections over the whole nuclear length were taken at several time points during cellularisation. To measure tub::GFP intensities, the respective plane at 50% nuclear

height for each recorded time point was chosen and analyzed using Metamorph. A field representing several nuclei was selected and the intensity of the tub::GFP signal was measured around each nucleus using linescans. Intensities in cytoplasmic regions were equally measured with linescans. Mean intensity values for each nucleus and cytoplasmic region were calculated and intensities were normalized to the sum of NE + cytoplasmic tub::GFP intensity for each respective time point. To quantify tub::GFP intensities after antibody injections, ratios between NE-attached and cytoplasmic tub::GFP intensities were calculated, in- or outside the WGA-labeled injection region respectively.

To measure the lifetime of MT-bundles, nuclei of tub::GFP expressing embryos were imaged on a confocal microscope for 100 seconds. Kymographs of tub::GFP along the NE were created using Metamorph and persistence times of bundles was measured from these kymographs in seconds.

To measure persistence times of H2Av::GFP spots, nuclei were imaged for 260 seconds on a confocal microscope. Kymographs spanning entire nuclear diameter were recorded using Metamorph and the length of tracks was measured in pixels and transformed in seconds.

To account for non Gaussian distribution of datasets, (two-tailed) p-values were calculated by Mann-Whitney U tests.

Photobleaching experiments

GFP photobleaching experiments were performed on a Zeiss 510 Meta confocal microscope. Images were acquired with a 100x/1.3 oil objective. A 488-nm Argon laser at 5.2μW photonic output power was used. After 10 pre-bleach images, twenty iterations at 100% transmission were used to photobleach circular regions of interests (ROI) between 1.6 to 6 μm^2. 0.75% transmission was used for image acquisition. Images were typically acquired at a pixel time of 6.4μs and a scan frame of 128x100 pixels for 100s. Fluorescence intensity on the bleached or control ROI was measured using the Metamorph software after correction for drift. Large regions including at least one nucleus were used as control regions. Raw fluorescence intensity measurements were background subtracted and normalized to arbitrary fluorescence units (pre-bleach time points normalized to one). Fluorescence recovery was calculated as the percentage of the bleached fluorescence obtained at a plateau. Curves were plotted using Excel (Microsoft) .

Isolation of Nuclei for AFM

Staged dechorionated embryos were lysed with a potter in Lysis Buffer (25 mM Tris, pH 8.0, 27.5 mM NaCl, 20 mM KCl, 25 mM Sucrose, 10 mM EDTA, 10 mM EGTA, 10% (v/v) Glycerol, 0.5% Nonidet P40). After removal of the debris, nuclei were isolated by centrifugation at 7000 rpm for 15 min. Nuclei were re-suspended in 20 μl of Lysis Buffer and seeded onto a chamber delimitated by a plastic ring on a Hellmanex and plasma activated microscope slide. Before seeding, chambers were pre-incubated with WGA-Alexa488 (20 mg/ml) for up to 2h. Nuclei were allowed to adhere for 30-45 min and subsequently washed with lysis buffer.

Atomic force microscopy

Mechanical experiments were conducted with an AFM (Nanowizard I, JPK Instruments, Berlin) mounted on an inverted fluorescence microscope (Zeiss Axiovert 200 equipped with 10x and 20x lens) [42]. The AFM head is equipped with a 15 μm z-range linearized piezoelectric ceramic scanner and an infrared laser. Bright-field imaging was used to select nuclei and monitor their morphology during force measurements. The setup was used in closed height feedback mode [43]. Before each experiment the sensitivity of the optical lever system was calibrated on glass

substrates and the cantilever spring constant was determined in situ using built-in routines of the JPK software by using the thermal noise method [Franz et al 2008]. Spring constants were found to be consistent with the manufacturer's nominal value (MSCT, Veeco Instruments – nominal constant 10pN/nm). Experiments were run at 25°C in lysis buffer for maximal 1 hour to minimize evaporation

Using the optical microscope, a calibrated cantilever was positioned over a chosen immobilized nucleus. The speed for putting or removing the tip from nuclei was set to 1µm/s and the desired contact force to 500 pN. 1024 points per sec were measured over a travel distance of 4 µm. The apparent contact time was set to 0 to minimize potential dissipation contributions. At least 10 successive force curves were obtained from each nucleus.

Each curve was examined by eye and processing was performed using the JPK-IP batch processing procedures: correcting for baseline shift and/or tilt for the pushing part of the force curve, finding the contact point between the tip and the nucleus, calculating the tip sample separation distance and fitting the pushing part of the force curve with the Hertz model [36] for a square based pyramid with an average half angle of 21° (calculated from the data of the provider). This last step allows us to gain the value of the Young modulus E (for a 1 µm/s speed and 500pN indenting force) for each measurement. E values for each nucleus were pooled to calculate median values and quartiles. No correlation was observed for successive force-curves on one nucleus nor for successive nuclei.

Particle Image Velocimetry

Images were analyses using the Particle Image Velocimetry free software program (MatPIV)(Sveen and Cowen, 2004) and MatLab. MatPIV analysis is based on cross-correlation of intensity of small bins between subsequent time frames. First MatPIV was applied to the whole image. The correction to the horizontal displacement was done by subtraction of the average velocity. Spatial masks were applied to filter out vectors outside nuclei or internal regions respectively. To obtain the masks fluorescent images were blurred by a Gaussian filter and the intensity threshold was applied for each image in the movie. The resulting velocitiy distributions were well fitted by a Gaussian distribution. For the comparison of different genotypes or conditions, mean velocities were calculated for each frame and subsequently averaged.

Author contributions

Experiments were designed by B.H., P.H.P. and T.L. Y.A performed all FRAP experiments and 3D reconstructions and participated in image analysis. R.F., P.H.P and B.H performed the AFM experiments, O.M did the PIV analysis and B.H. did all other experiments. The manuscript was written by B.H., P.H.P. and T.L.

Figure Legends

Fig 1: Microtubules control NE morphogenesis during *Drosophila* cellularisation

a-c: Microtubules regulate NE-shape. **a**: 3D reconstruction from serial z sections of a nucleus from a wt embryo imaged 10 or 45 minutes after mitosis 13. **b,b',b''**: Top-view stills from time lapse movies of wild type embryos injected with WGA Alexa-488 showing round (b), polygonal (b') or grooved nuclei (b''). Indicated times refer to the start of interphase 14. **c,c',c''**: Top view stills of wild type embryos injected with Colcemid and WGA Alexa-488. Indicated times refer to the start of interphase 14. Schematics depict NE arrangements. **d-f**: MTs accumulate at the NE during cellularisation. **d**: Schematic representation of MT organization during cellularisation in a sagital view. **e**: Top-view stills from a time-lapse movie of a tub::GFP expressing embryo during cellularisation. Indicated times refer to start of interphase 14. Note the pronounced accumulation of tub::GFP in grooves (arrowheads). **f**: Quantification of normalized tub::GFP at the NE or in the cytoplasm for 3 embryos. Plotted are mean intensities of 6 nuclei for each embryo. **g:** Quantification of normalized alpha-tubulin levels at the NE or in the cytoplasm based on antibody stainings on fixed wild type embryos in late cellularisation (p=7.29 x 10^{-4}, n=4 embryos, 44 nuclei, 53 cytoplasmic regions). **h-j**: NE-dynamics and groove formation depends on MTs. NE-deformations are measured as the distance between the most lateral positions of the signal from WGA-Alexa 488 kymographs (h',i') from time lapse movies of wild type (h,h) or Colcemid injected embryos (i,i'') over a period of 6 min. One respective frame is shown in h,i. Scalebars in (h',i') are 1µm and the indicated times in (h,i) refer to the start of interphase 14. Note the reversibility of groove formation (h'). j: NE-fluctuations are different in nuclei from either younger (n=9) or older (n=14) cellularising embryos or between wild type or Colcemid treated embryos (n=8), respectively.

Fig 2: Dynamic Microtubules are organized in stationary bundles at the NE

a,b: MTs occur in bundles along the NE. Top-view stills (a,b) and kymographs (a',b') from time lapse movies of tub::GFP expressing embryos, before (a,a') or after (b,b') groove formation. The tub::GFP signal was recorded over 100 seconds. MT-bundles are indicated by arrowheads (a'b'). **c-e**: A subset of MTs along the NE is acetylated and decorates grooves. Top views from fixed wild type embryos during cellularisation (c,d). Acetyl-Tubulin marks a subset of the total MT population (c) and is distributed along the NE (d). **e**. Quantification of the percentage of grooves and lobules, which are occupied by an acetyl-tub spot, as counted from images like (d). **f-,g**: MTs within bundles are dynamic and grow in an apical-basal direction. Intensity curves (f') and kymograph (f'') of tub::GFP in a control (grey) or photobleached (red) half of a nucleus of a cellularising embryo expressing tub::GFP (f), followed over 100 seconds. The region depicted in the kymograph is indicated by the orange bar in (f). Tub::GFP recovery derives from MT-polymerisation in an apical-basal direction without any lateral sliding from the control region (f') and without any intensity loss within the control half of the nucleus (f') **g**: Recovery fractions of tub::GFP after FRAP are similar between embryos in early (n=7 nuclei) or late cellularisation and between grooves (n=5) and non grooves (n=8) respectively.

Fig 3: Dynamic MTs trigger nuclear morphogenesis

a, a': : Two modes characterize NE dynamics. Besides the large scale deformations indicated by the distance between the most lateral positions in the NE kymograph over 6 min (a), high-frequency NE-fluctuations are measured as standard deviations (STDV) σ of the positions of the lateral intensity maxima from WGA-Alexa 488 kymographs (indicated by the black line following the signal in a') recorded over 1 min intervals with a frame every 5 seconds. Scalebar =1μm. **b**: NE dynamics starts with cellularisation and depends on MTs. Histogram of STDV from NE-fluctuations for wild type in Interphase 14 (n=204 1min intervalls) and Interphase 13 (n=135) and from Colcemid injected cellularising embryos (n=114). **c,d**: Taxol injection reduces MT dynamics. Top view stills (c,c') from a time lapse movie of embryos expressing EB1::GFP injected with solvent (c) or taxol (c'), where EB1::GFP levels are strongly reduced at the NE. **d**: Typical recovery curves after FRAP from a control or taxol injected tub::GFP expressing embryo. **e**: Impaired MT dynamics reduces high-frequency fluctuations of the NE. Histogram of the STDV from high frequency NE-fluctuations in DMSO (n=150 1 min intervals) or Taxol injected (n=149) cellularising embryos. **f-g**: MT bundles are stabilized upon Taxol injection. Kymographs (f,f') from a tub::GFP expressing control (f) or taxol (f') injected embryo imaged for 100 sec. Scalebar =1μm. **g**: Lifetimes of MT-bundles are measured from kymographs recorded in tub::GFP expressing embryos and presented as a histogram comparing bundle-lifetimes in control (n=166 bundles) or taxol (n=87) injected embryos. **h-j**: Blocking MT dynamics impairs NE groove formation. Top view stills (h-i") from embryos co-injected with WGA-Alexa 488 and either DMSO (h, h', h") or Taxol (i, i', i"). Indicated time points refer to t1 in (h,i). **j**: Comparison of large scale NE-deformations indicating groove formation at similar times after mitosis in controls (n=10) or Taxol injected embryos (n=9) (p=1.57 x 10^{-4}).

Fig 4: Cytoplasmic Dynein Bundles Microtubules at the Nuclear Envelope

a-c: MT's are reduced at the NE upon Dynein de-activation. Top-view stills from a movie recording a tub-GFP expressing embryo co-injected with α-Dhc antibody and WGA-Alexa555 (a,b). Out/inside distinction is based on the presence of WGA-Alexa555 (a). Quantification of tub::GFP levels around the NE and in the cytoplasm (c). Plotted are the ratios of NE attached / cytoplasmic tub::GFP out- respectively inside the injection area after injection with the respective antibodies. **d-f**: Dynein impairment does not reduce MT-growth. Top view still from a time lapse movie recording an embryo expressing EB1::GFP after co-injection with α-Dhc antibody and WGA-Alexa555 (d). Quantification (e) of EB1::GFP spots counted per μm NE reveals no difference either in-or outside the α-Dhc antibody/WGA injection area (n= 50 nuclei in 4 embryos, p=0.114). **f**: MT-polymerisation dependant high-frequency NE oscillations are similar between wild type (n=204 1 min intervals)) and α-Dhc + α-Dic (n=186) injected embryos. **g,h**: Dynein controls integrity of MT bundles at the NE. Tub::GFP Kymographs (g,g',g") recorded over 100 seconds from either α-Dhc (g,g') or α-GST (g") antibody injected embryos. **h**: Histogram of MT-bundle lifetimes at the NE inside (n=388 bundles) or outside (n=177 bundles) the α-Dhc antibody targeted region, as measured from kymographs like in g,g'. **i-l**: Dynein inhibition affects nuclear morphogenesis. Top view stills (i,i',j,j',k,k') and kymographs (i",j",k") of NE's from either α-GST (i,i',i"), α-Dhc (j,j',j") or α-DIC (k,k',k") antibody injected embryos. The indicated times refer to the start of interphase 14. **l**: Comparison of large scale NE-deformations about 30 min after start of interphase 14 between α-GST (n=9), α-Dhc (n=10) or α-DIC (n=15) antibody injected embryos (α-GST/α-Dhc: p=2.39 x10^{-4}; α-GST/α-DIC: p=5.7 x 10^{-5}).

Fig 5: The farnesylated protein Char/Kuk mediates MT induced nuclear deformation

a-d: Farnesylated INM proteins and nuclear morphology. Top view stills taken at a medial z plane from embryos of the respective genotypes injected with WGA-Alexa488. Indicated times refer to entry into Interphase 14. **a,b**: Char/Kuk is required for NE deformation (a,a',a''), and its over-expression leads to stronger and premature NE lobulation (b,b',b''). **c,d**: Dm0 over-expression does not phenocopy *char/kuk* expression (c,c',c'') and cannot rescue the lobulation defects in *char/kuk* mutants (d,d',d''). **e-g**: Farnesylated INM proteins regulate NE elasticity. e,e': NE-Elasticity can be measured by AFM on isolated nuclei. **e**: Typical pressing force curve with a Hertz fit for a pyramidal intender (white line) for an isolated nucleus. For a given pressing force F the Young Modulus E is inversely proportional to the square of the indentation σ. **e'**: Photomicrograph of an AFM cantilever close to a single immobilized nucleus. Scale-bar = 20µm. **f**: Whisker plots of E-moduli measured for nuclei isolated from embryos of the indicated genotypes and developmental stages **g**: Force dissipation curves after pressing on isolated nuclei of the respective genotypes over 10 seconds. **h-k:** Char stabilizes MT induced NE deformations. **h**: Schematics and top view stills from two z planes of the same nucleus from a wild type embryo injected with WGA-Alexa488 and Colcemid about 15-10 min after mitosis 13. **i,j**: Top view stills from 6xchar/kuk embryos injected with WGA-Alexa488, either before (i,j) or after (i',i'', j', j'') subsequent Colcemid injection. Colcemid treatment soon after mitosis (i', i'') abolishes MT induced NE deformation and shows buckling due to lateral nuclear growth, MT de-polymerization slightly later during cellularisation (j',j'') deforms the NE similar to wild type. Indicated time points refer to Colcemid injection. **k:** NE grooves progress independent of MTs. Top view stills of a 6xchar/kuk embryo injected with WGA-Alexa488 and after Colcemid treatment during mid-cellularization, once grooves were already initiated. Asterisks follow distinct grooves, which get more pronounced over subsequent frames. Time points in (k',k'') correspond to minutes after t1(k).

Fig.6: NE dynamics induces chromatin mobility

Chromatin is dynamic in cellularising *Drosophila* embryos. **a,a'**:Top view still (a) and kymograph (a') from a time lapse movie imaging one z-plane sectioned through nuclei of a cellularising embryo expressing H2Av::GFP and injected with WGA-Alexa555. H2Av::GFP is diffuse throughout nuclei and concentrates in spots which can be tracked in kymographs. The region depicted in the kymograph corresponds to the orange bar in (a). **a'**: H2Av::GFP spots move parallel to NE deformations adjacent to the NE (filled arrowheads) but also in the nuclear interior (open arrowhead) or move independently of the NE track (asterisk). **b,c,c'**: Analysis of Chromatin dynamics by PIV. **b**: Representation of a nucleus from a H2Av::GFP expressing IP14 control embryo with the corresponding vector-field determined for 2 subsequent frames. The H2Av::GFP signal is pseudo-colored. **c,c'**: Chromatin velocities are decreased when NE dynamics is reduced or morphogenesis is inhibited. **c**: Mean H2Av::GFP velocities calculated for whole nuclei are significantly higher in control IP14 embryos (99 PIVs from 6 embryos) than in Colcemid injected embryos (87 PIVs, 5 embryos, $p=4.7 \times 10^{-28}$), char/kuk RNAi depleted embryos (66 PIVs, 5 embryos, $p=1.7 \times 10^{-7}$), or IP 13 embryos (43 PIVs, 4 embryos, $p=4.23 \times 10^{-14}$). **c'**: PIV analysis of H2Av::GFP in central parts of nuclei. Mean velocities in control IP14 embryos are higher than in Colcemid treated ($p=5.17 \times 10^{-26}$), char/kuk RNAi ($p=5.11 \times 10^{-7}$) or wild type IP13 embryos ($p=2.38 \times 10^{-5}$). **d-g**: Kymographs of H2AvGFP in one respective nucleus imaged for 260 seconds at one medial z plane. ROIs for kymographs were chosen as indicated in the scheme. H2Av::GFP spots

appear short-lived in nuclei from control Interphase 14 embryos (d), while they often form tracks spanning the entire movie in IP13 nuclei (e), upon Colcemid injection(f) or RNAi depletion of *char/kuk* (g). **h,h':** Histograms of the residence times of H2Av::GFP spots quantified as indicated by the grey vertical bars in (d). H2Av::GFP spots from wild type IP14 nuclei (333 spots from 5 embryos) stay significantly shorter than in nuclei from wild type IP13 embryos (222 spots, 4 embryos, p=8.79 x 10^{-27}), Colcemid injected embryos (300 spots, 5 embryos, p=2.17 x 10^{-15}) or *char/kuk* RNAi (195 spots, 5 embryos, p=6.89 x 10^{-12}).

Supplementary Information

Fig S1: Nuclear morphogenesis during *Drosophila* cellularisation

a: Normalized surface growth of four wild type embryos after mitosis 13. Plotted values were calculated from 3D reconstructions based on serial z sections and represent the means of 6 nuclei per embryo for each time point. Highlighted is the transition from a polygonal to a lobulated geometry and the corresponding mean value for the surface increase. **b,b':** Nuclei change shape independent of the ingressing Plasma membrane. Top view stills of a time lapse movie imaging an embryo expressing a GFP fusion protein of the regulatory light chain of Myosin II, Spaghetti squash (Sqh::GFP), which labels the furrow canal at the tip of the ingressing plasma membrane. The embryo was injected with *slam* dsRNAi and WGA-Alexa555 and shows the same irregular NE- morphology at the z-plane corresponding to the furrow canal (b) and 4µm below (b').

Fig S2: Microtubules control nuclear elongation and surface increase

a: Normalized Surface increase in wild type and colcemid injected embryos. Surfaces are calculated from 3D reconstructions based on serial confocal z-sections. **b**: Nuclei elongate less in Dynein compromised cellularising embryos, where MTs at the NE are reduced. Represented values are means of 6 nuclei / time point.

Fig S3: Char/ Kuk Regulates Nuclear Morphogenesis Independent of Microtubules

a,-c: MT dynamics is unchanged when Char/Kuk is impaired. Recovery curve (a) and corresponding kymograph (a') for tub::GFP in a *char/kuk* dsRNAi injected embryo after FRAP. Recovery fractions of tub::GFP (b) are not different between wild type (n=18) and *char/kuk RNAi* injected embryos (n=12). **c**: High frequency fluctuations of the NE are similar in *char/kuk* embryos (n=126 1 minute intervals) compared to wild type (n=204) embryos (p= 9.24 x 10^{-2}).

Fig S4: Histone spot mobility along the apical-basal nuclear axis

a: z-series of kymographs spanning one nucleus taken from time lapse movies of H2Av::GFP expressing embryos during cellularisation. Represented kymographs are from the same nucleus in 1 μm distances, as schematically indicated.

Fig S5: NE morphogenesis affects Chromatin organization

a-e: sagital views of fixed embryos stained with anti-HP-1 and anti-H3K4Me2 antibodies. HP-1 concentrates apically during cellularisation (b,b'), compared to Interphase13 (a,a'). In Colcemid injected (c,c') or *char/kuk* mutat embryos, apical concentration of HP-1 is less pronounced and HP-1 labeled chromatin overlaps with active H3K4Me2 labeled chromatin (c,d,e). In *char/kuk* mutants this is not only

appearant one nuclei round up (e) but also before when nuclei undergo normal elongation (d).

References

1. Dahl, K. N., Ribeiro, A. J. & Lammerding, J. Nuclear shape, mechanics, and mechanotransduction. Circ Res 102, 1307-18 (2008).
2. Dauer, W. T. & Worman, H. J. The nuclear envelope as a signaling node in development and disease. Dev Cell 17, 626-38 (2009).
3. Brandt, A. et al. Developmental control of nuclear size and shape by Kugelkern and Kurzkern. Curr Biol 16, 543-52 (2006).
4. Pilot, F., Philippe, J. M., Lemmers, C., Chauvin, J. P. & Lecuit, T. Developmental control of nuclear morphogenesis and anchoring by charleston, identified in a functional genomic screen of Drosophila cellularisation. Development 133, 711-23 (2006).
5. Stuurman, N., Heins, S. & Aebi, U. Nuclear lamins: their structure, assembly, and interactions. J Struct Biol 122, 42-66 (1998).
6. Dechat, T. et al. Nuclear lamins: major factors in the structural organization and function of the nucleus and chromatin. Genes Dev 22, 832-53 (2008).
7. Pajerowski, J. D., Dahl, K. N., Zhong, F. L., Sammak, P. J. & Discher, D. E. Physical plasticity of the nucleus in stem cell differentiation. Proc Natl Acad Sci U S A 104, 15619-24 (2007).
8. Lammerding, J. et al. Lamin A/C deficiency causes defective nuclear mechanics and mechanotransduction. J Clin Invest 113, 370-8 (2004).
9. Schejter, E. D. & Wieschaus, E. Functional elements of the cytoskeleton in the early Drosophila embryo. Annu Rev Cell Biol 9, 67-99 (1993).
10. Edgar, B. A., Odell, G. M. & Schubiger, G. Cytoarchitecture and the patterning of fushi tarazu expression in the Drosophila blastoderm. Genes Dev 1, 1226-37 (1987).
11. Riemer, D. et al. Expression of Drosophila lamin C is developmentally regulated: analogies with vertebrate A-type lamins. J Cell Sci 108 (Pt 10), 3189-98 (1995).
12. Brandt, A., Krohne, G. & Grosshans, J. The farnesylated nuclear proteins KUGELKERN and LAMIN B promote aging-like phenotypes in Drosophila flies. Aging Cell 7, 541-51 (2008).
13. Polychronidou, M., Hellwig, A. & Grosshans, J. Farnesylated nuclear proteins Kugelkern and lamin Dm0 affect nuclear morphology by directly interacting with the nuclear membrane. Mol Biol Cell 21, 3409-20.
14. Rudolph, T. et al. Heterochromatin formation in Drosophila is initiated through active removal of H3K4 methylation by the LSD1 homolog SU(VAR)3-3. Mol Cell 26, 103-15 (2007).
15. Onischenko, E. A., Gubanova, N. V., Kieselbach, T., Kiseleva, E. V. & Hallberg, E. Annulate lamellae play only a minor role in the storage of excess nucleoporins in Drosophila embryos. Traffic 5, 152-64 (2004).
16. Lecuit, T., Samanta, R. & Wieschaus, E. slam encodes a developmental regulator of polarized membrane growth during cleavage of the Drosophila embryo. Dev Cell 2, 425-36 (2002).

17. Olins, A. L. & Olins, D. E. Cytoskeletal influences on nuclear shape in granulocytic HL-60 cells. BMC Cell Biol 5, 30 (2004).

18. Wolf, N., Regan, C. L. & Fuller, M. T. Temporal and spatial pattern of differences in microtubule behaviour during Drosophila embryogenesis revealed by distribution of a tubulin isoform. Development 102, 311-24 (1988).

19. Gonczy, P., Pichler, S., Kirkham, M. & Hyman, A. A. Cytoplasmic dynein is required for distinct aspects of MTOC positioning, including centrosome separation, in the one cell stage Caenorhabditis elegans embryo. J Cell Biol 147, 135-50 (1999).

20. Robinson, J. T., Wojcik, E. J., Sanders, M. A., McGrail, M. & Hays, T. S. Cytoplasmic dynein is required for the nuclear attachment and migration of centrosomes during mitosis in Drosophila. J Cell Biol 146, 597-608 (1999).

21. Beaudouin, J., Gerlich, D., Daigle, N., Eils, R. & Ellenberg, J. Nuclear envelope breakdown proceeds by microtubule-induced tearing of the lamina. Cell 108, 83-96 (2002).

22. Salina, D. et al. Cytoplasmic dynein as a facilitator of nuclear envelope breakdown. Cell 108, 97-107 (2002).

23. Han, G. et al. The Aspergillus cytoplasmic dynein heavy chain and NUDF localize to microtubule ends and affect microtubule dynamics. Curr Biol 11, 719-24 (2001).

24. Lammerding, J., Dahl, K. N., Discher, D. E. & Kamm, R. D. Nuclear mechanics and methods. Methods Cell Biol 83, 269-94 (2007).

25. Clarkson, M. & Saint, R. A His2AvDGFP fusion gene complements a lethal His2AvD mutant allele and provides an in vivo marker for Drosophila chromosome behavior. DNA Cell Biol 18, 457-62 (1999).

26. Laan, L., Husson, J., Munteanu, E. L., Kerssemakers, J. W. & Dogterom, M. Force-generation and dynamic instability of microtubule bundles. Proc Natl Acad Sci U S A 105, 8920-5 (2008).

27. Patterson, K. et al. The functions of Klarsicht and nuclear lamin in developmentally regulated nuclear migrations of photoreceptor cells in the Drosophila eye. Mol Biol Cell 15, 600-10 (2004).

28. Malone, C. J. et al. The C. elegans hook protein, ZYG-12, mediates the essential attachment between the centrosome and nucleus. Cell 115, 825-36 (2003).

29. Zhou, K., Rolls, M. M., Hall, D. H., Malone, C. J. & Hanna-Rose, W. A ZYG-12-dynein interaction at the nuclear envelope defines cytoskeletal architecture in the C. elegans gonad. J Cell Biol 186, 229-41 (2009).

30. Burke, B. & Roux, K. J. Nuclei take a position: managing nuclear location. Dev Cell 17, 587-97 (2009).

31. Hiraoka, Y. & Dernburg, A. F. The SUN rises on meiotic chromosome dynamics. Dev Cell 17, 598-605 (2009).

32. King, M. C., Drivas, T. G. & Blobel, G. A network of nuclear envelope membrane proteins linking centromeres to microtubules. Cell 134, 427-38 (2008).

33. Chikashige, Y., Haraguchi, T. & Hiraoka, Y. Another way to move chromosomes. Chromosoma 116, 497-505 (2007).

34. Osborne, C. S. et al. Active genes dynamically colocalize to shared sites of ongoing transcription. Nat Genet 36, 1065-71 (2004).

35. Bantignies, F. et al. Polycomb-Dependent Regulatory Contacts between Distant Hox Loci in Drosophila. Cell 144, 214-26.

36. Schape, J., Prausse, S., Radmacher, M. & Stick, R. Influence of lamin A on the mechanical properties of amphibian oocyte nuclei measured by atomic force microscopy. Biophys J 96, 4319-25 (2009).

37. Gruenbaum, Y., Margalit, A., Goldman, R. D., Shumaker, D. K. & Wilson, K. L. The nuclear lamina comes of age. Nat Rev Mol Cell Biol 6, 21-31 (2005).

38. Jankovics, F. & Brunner, D. Transiently reorganized microtubules are essential for zippering during dorsal closure in Drosophila melanogaster. Dev Cell 11, 375-85 (2006).

39. Sharp, D. J., Rogers, G. C. & Scholey, J. M. Cytoplasmic dynein is required for poleward chromosome movement during mitosis in Drosophila embryos. Nat Cell Biol 2, 922-30 (2000).

40. Cavey, M. & Lecuit, T. Imaging cellular and molecular dynamics in live embryos using fluorescent proteins. Methods Mol Biol 420, 219-38 (2008).

41. Tassy, O., Daian, F., Hudson, C., Bertrand, V. & Lemaire, P. A quantitative approach to the study of cell shapes and interactions during early chordate embryogenesis. Curr Biol 16, 345-58 (2006).

42. Puech, P. H. et al. Measuring cell adhesion forces of primary gastrulating cells from zebrafish using atomic force microscopy. J Cell Sci 118, 4199-206 (2005).

43. Puech, P. H., Poole, K., Knebel, D. & Muller, D. J. A new technical approach to quantify cell-cell adhesion forces by AFM. Ultramicroscopy 106, 637-44 (2006).
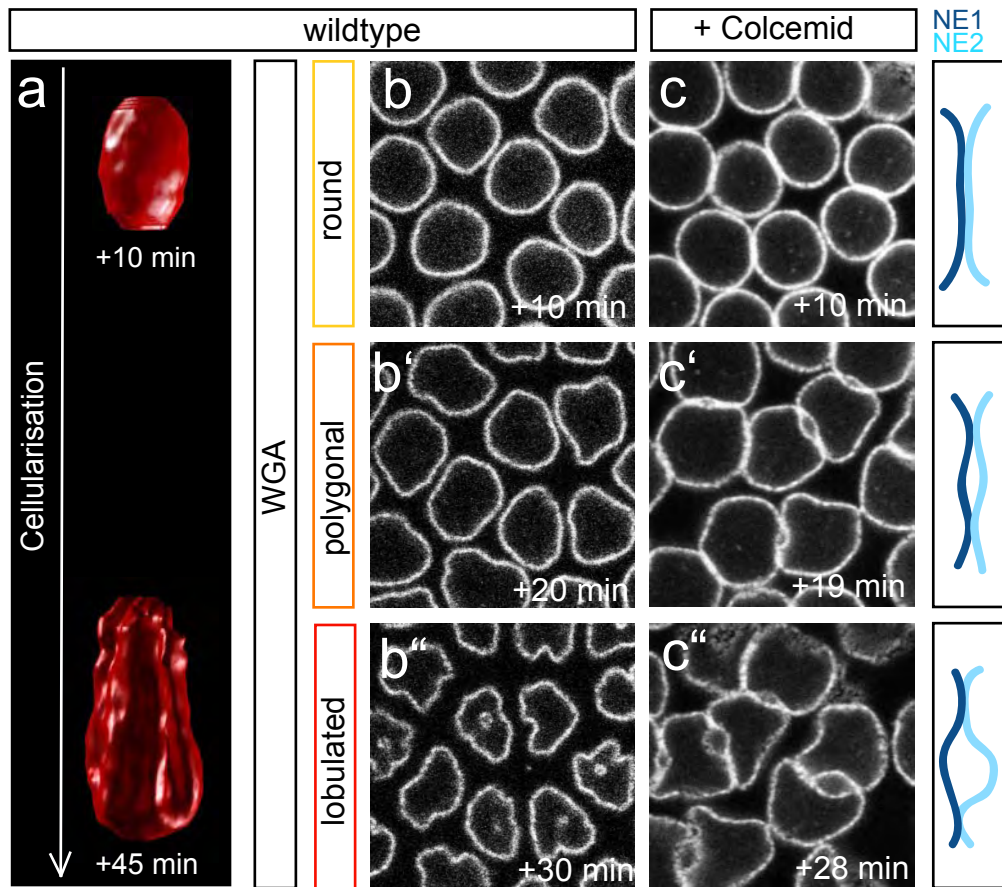
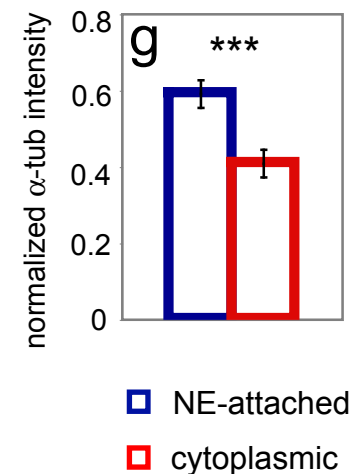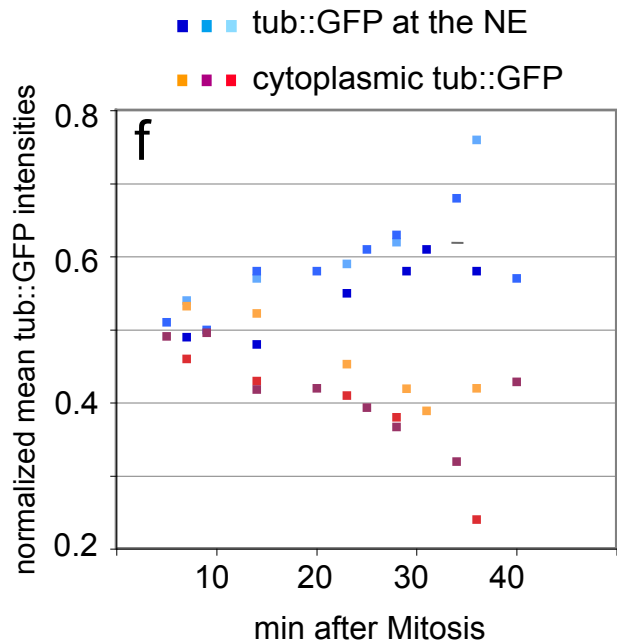Fig 1: Microtubules control nuclear morphogenesis during *Drosophila* cellularisation
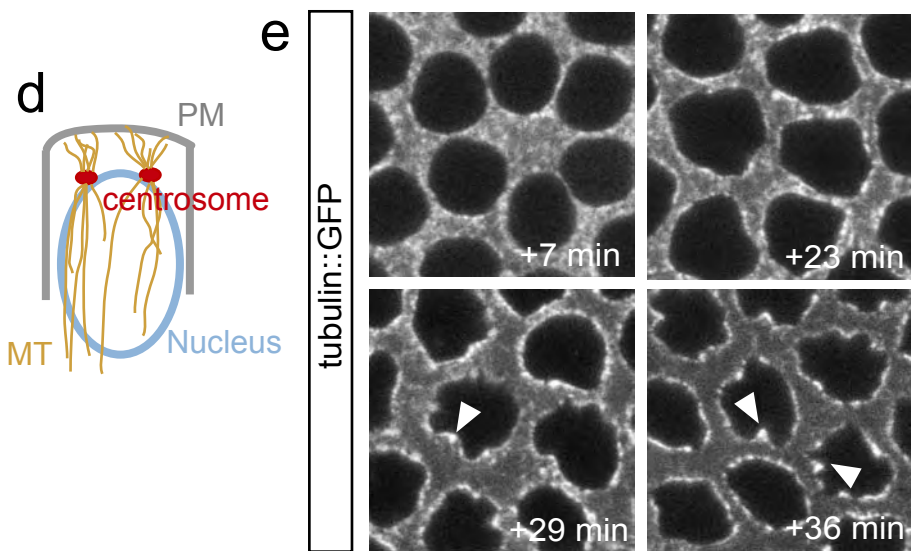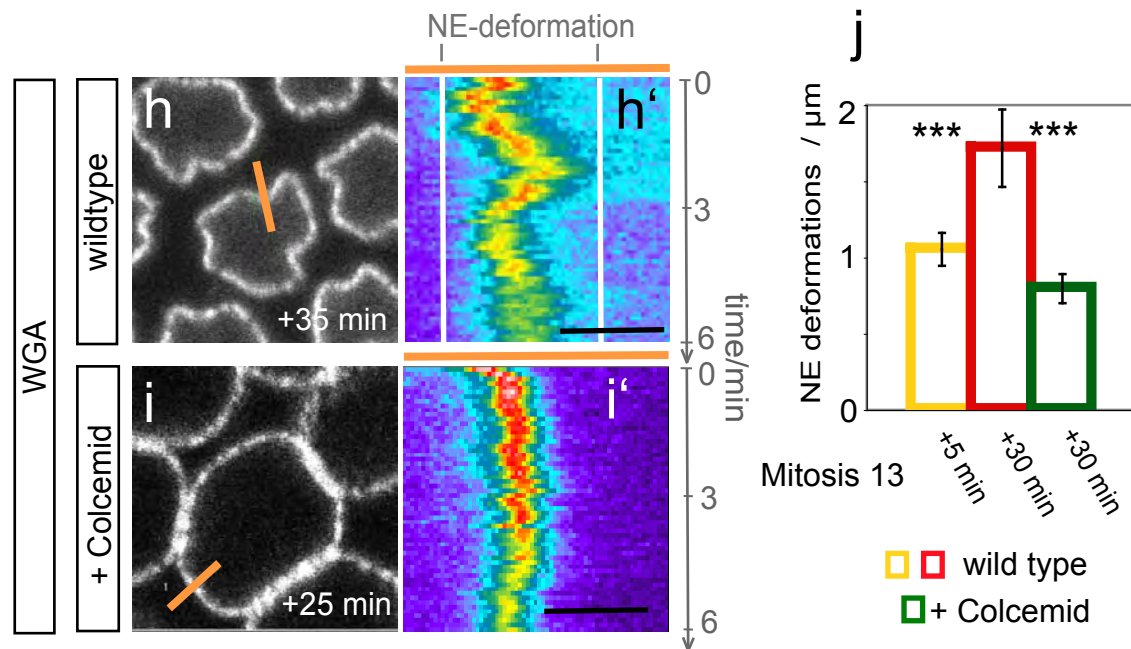
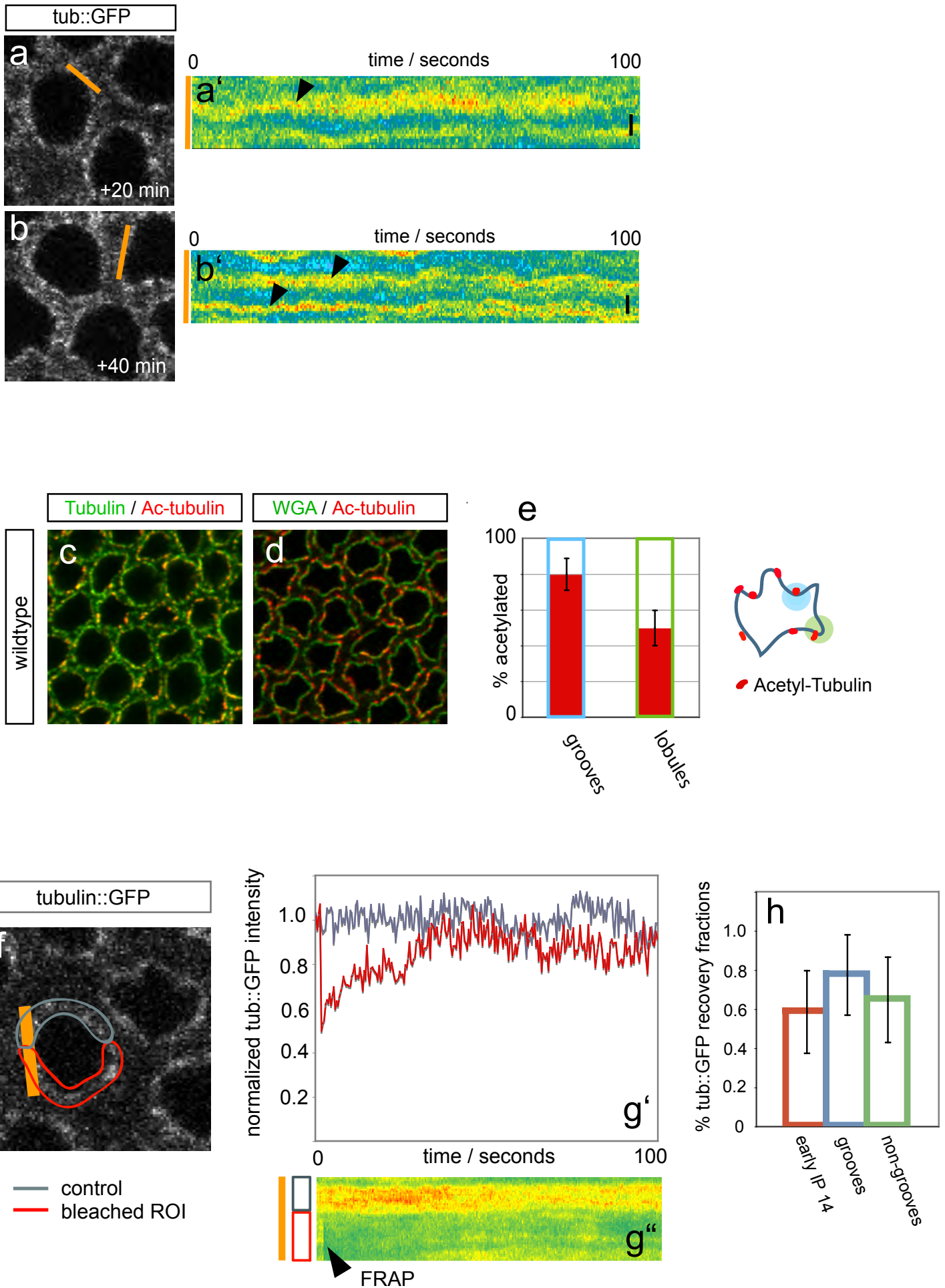Fig 2: Dynamic Microtubules Are Organized within Stationary Bundles at the NE

tub::GFP

a +20 min

time / seconds 0 — 100

a'

b +40 min

time / seconds 0 — 100

b'

wildtype

Tubulin / Ac-tubulin

c

WGA / Ac-tubulin

d

e

% acetylated

grooves   lobules

Acetyl-Tubulin

tubulin::GFP

f

control
bleached ROI

normalized tub::GFP intensity

time / seconds

g'

g''

FRAP

h

% tub::GFP recovery fractions

eatly IP 14   grooves   non-grooves

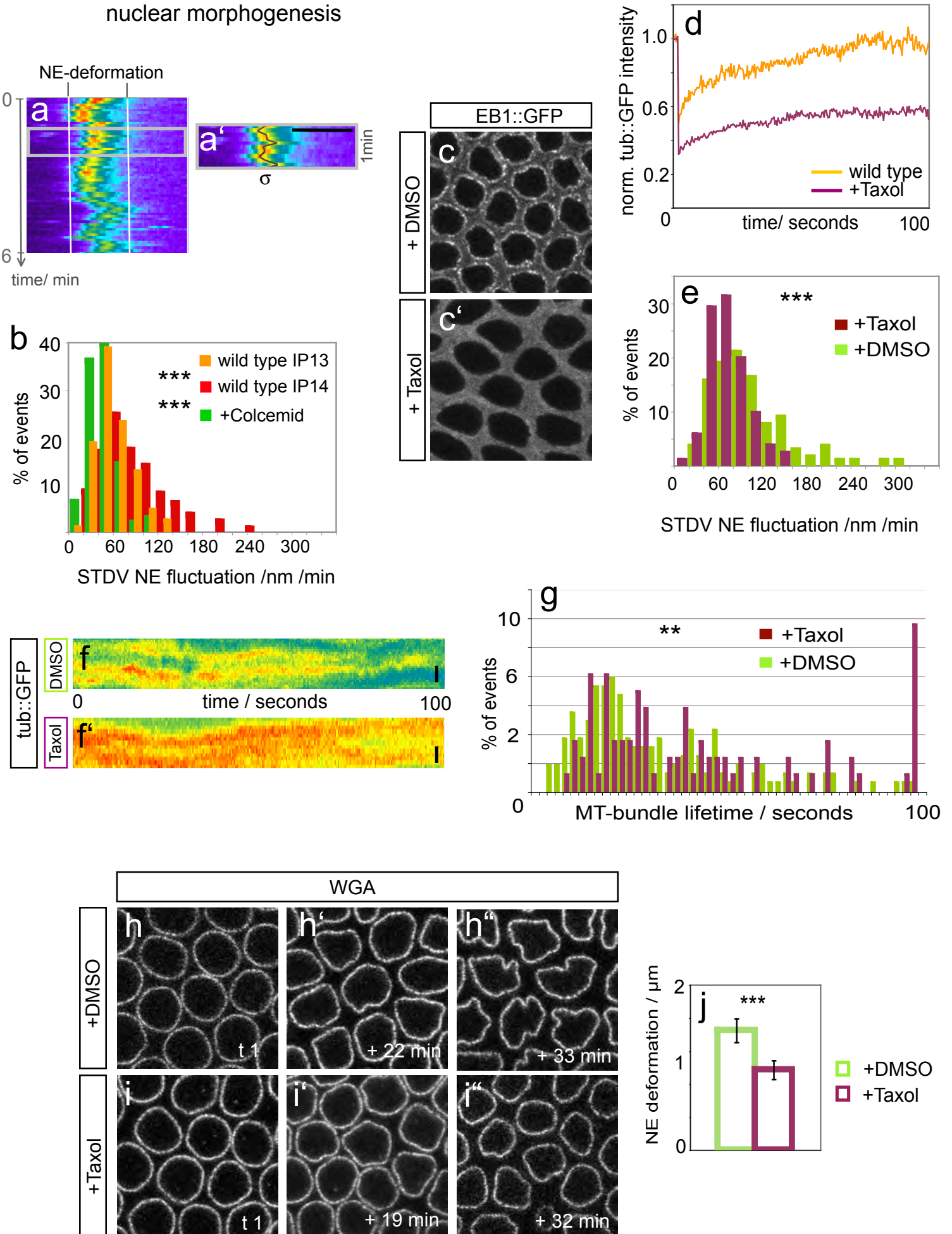Figure 3: Microtubule dynamics trigger nuclear morphogenesis

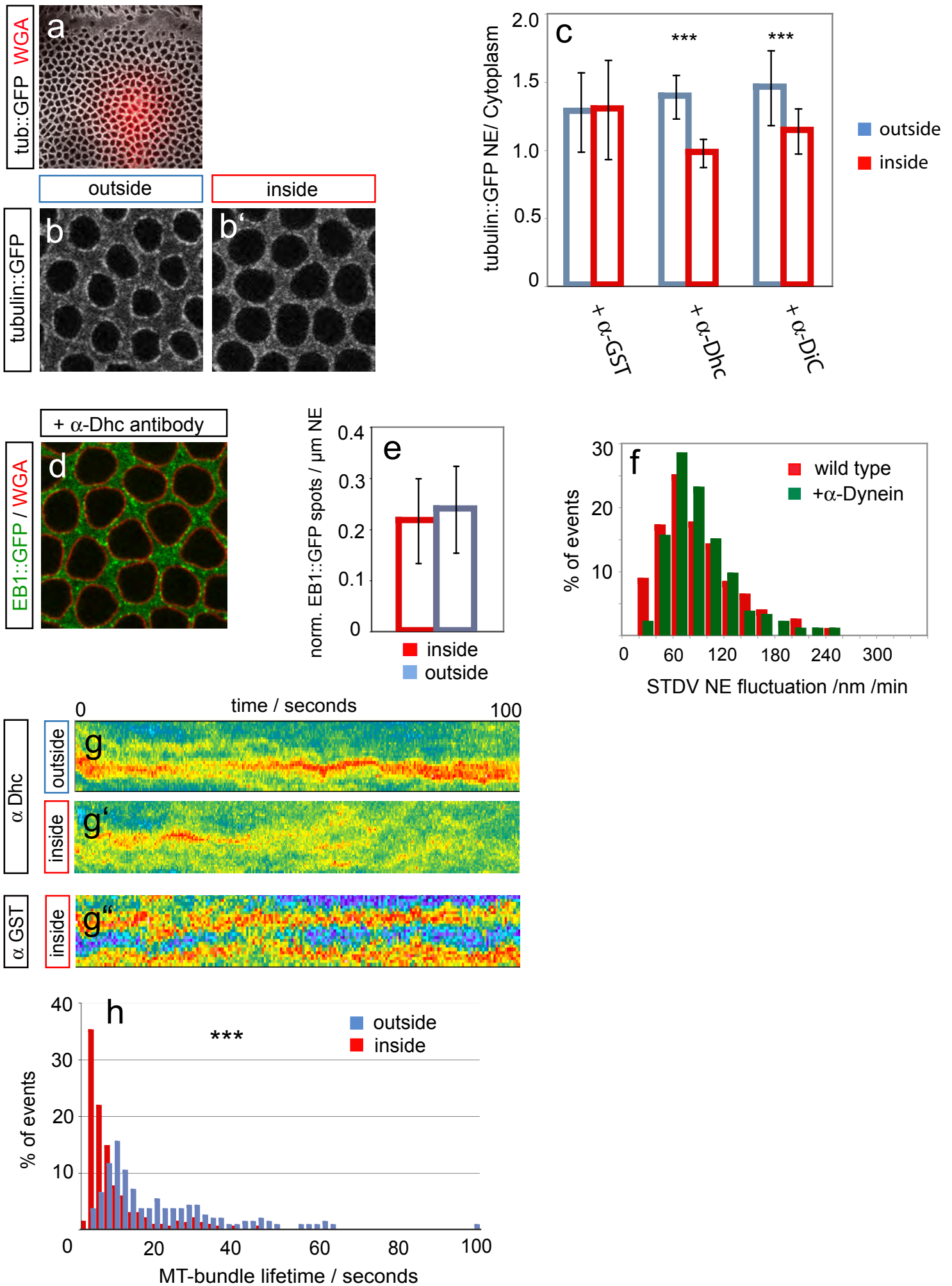Figure 4: Cytoplasmic Dynein bundles Microtubule at the Nuclear Envelope

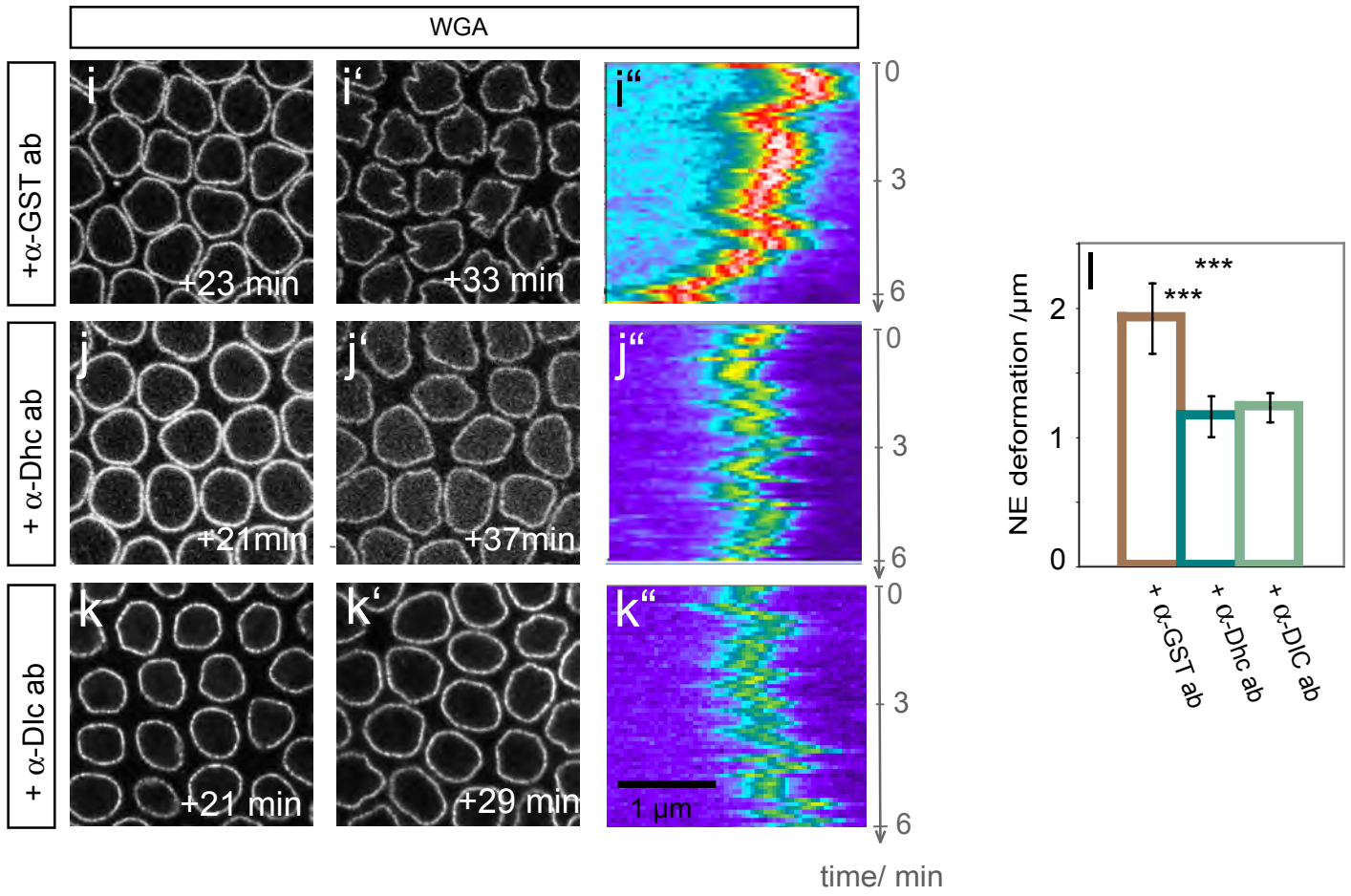# Fig.4: Cytoplasmic Dynein Bundles Microtubules at the Nuclear Envelope

Figure 5: The NE protein Char/Kuk mediates Microtubule induced nuclear morphogenesis
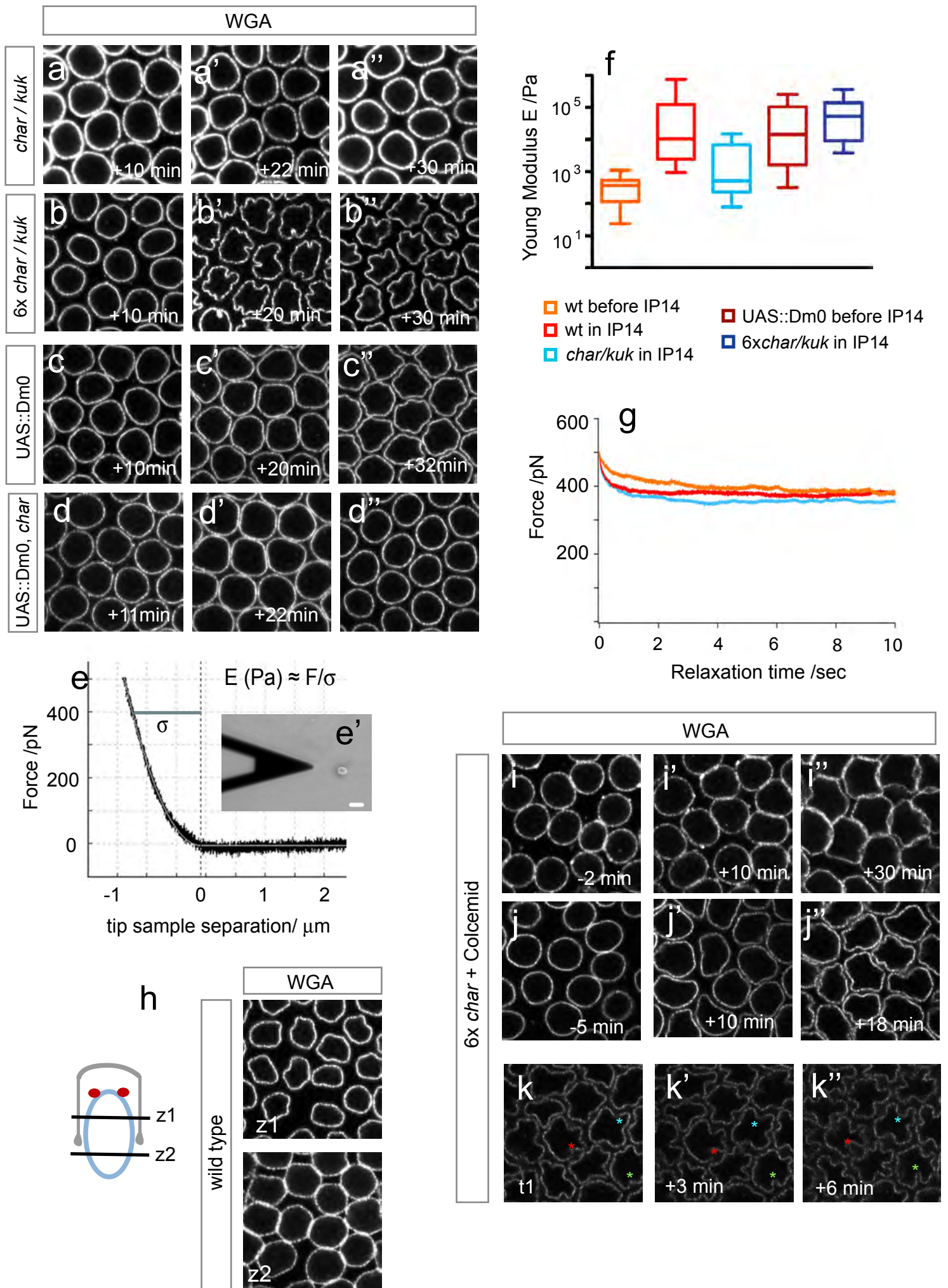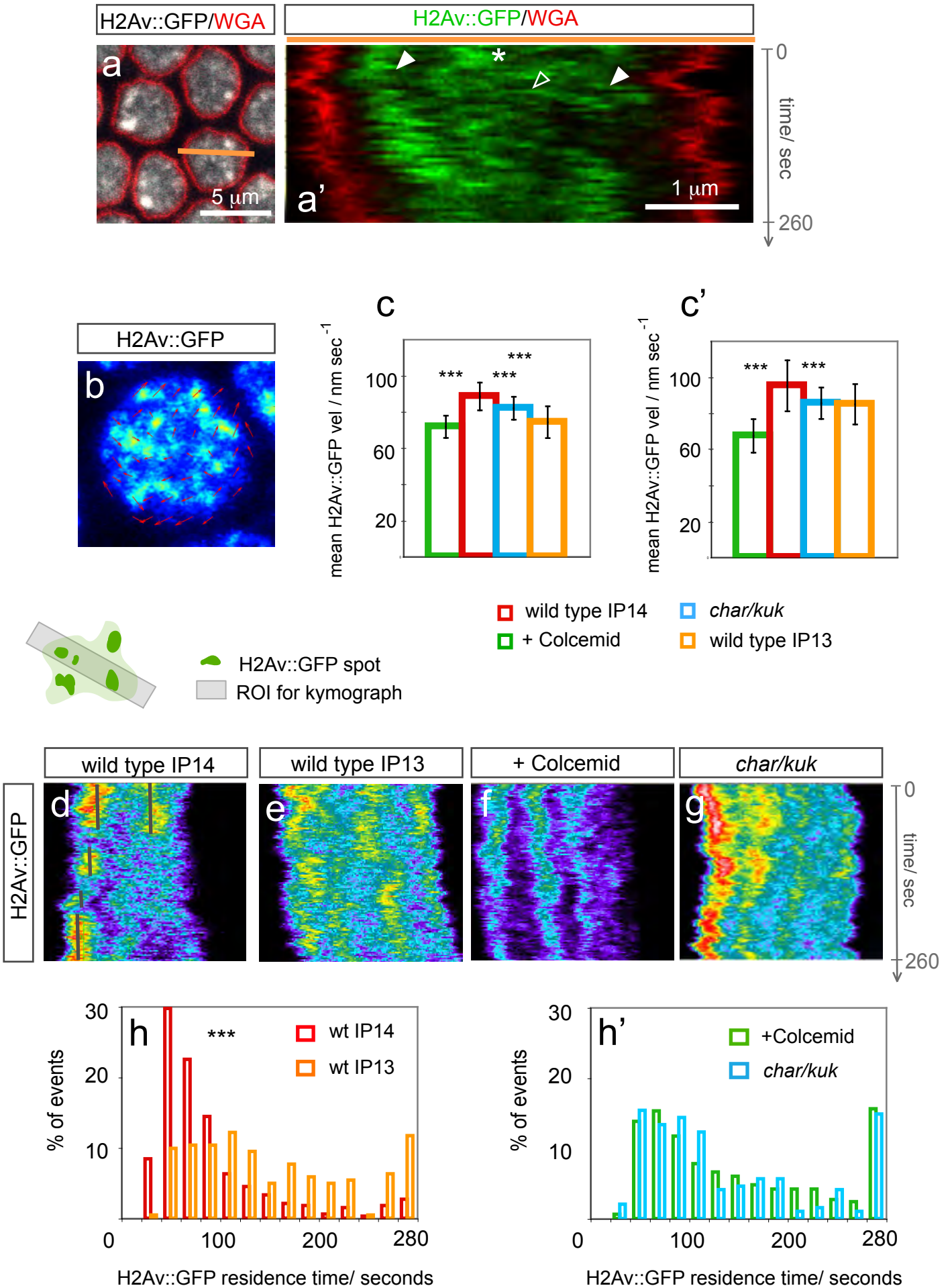

WGA

char / kuk

a +10 min a' +22 min a'' +30 min

6x char / kuk

b +10 min b' +20 min b'' +30 min

UAS::Dm0

c +10min c' +20min c'' +32min

UAS::Dm0, char

d +11min d' +22min d''

f

Young Modulus E /Pa

□ wt before IP14   □ UAS::Dm0 before IP14
□ wt in IP14   □ 6xchar/kuk in IP14
□ char/kuk in IP14

g

Force /pN

Relaxation time /sec

e

$E (Pa) \approx F/\sigma$

Force /pN

σ

e'

tip sample separation/ μm

h

WGA

z1
z2

wild type

z1

z2

WGA

6x char + Colcemid

i -2 min i' +10 min i'' +30 min

j -5 min j' +10 min j'' +18 min

k t1 k' +3 min k'' +6 min

Figure 6: Nuclear envelope dynamics induces Chromatin Mobility

H2Av::GFP/WGA

a

5 µm

H2Av::GFP/WGA

a'

0

time/ sec

260

1 µm

H2Av::GFP

b

c

mean H2Av::GFP vel / nm sec^{-1}

100

60

20

*** *** ***

c'

mean H2Av::GFP vel / nm sec^{-1}

100

60

20

*** ***

□ wild type IP14   □ char/kuk
□ + Colcemid   □ wild type IP13

● H2Av::GFP spot
▨ ROI for kymograph

wild type IP14   wild type IP13   + Colcemid   char/kuk

d   e   f   g

H2Av::GFP

0

time/ sec

260

h

30

20

10

% of events

*** □ wt IP14 □ wt IP13

0   100   200   280

H2Av::GFP residence time/ seconds

h'

30

20

10

% of events

□ +Colcemid □ char/kuk

0   100   200   280

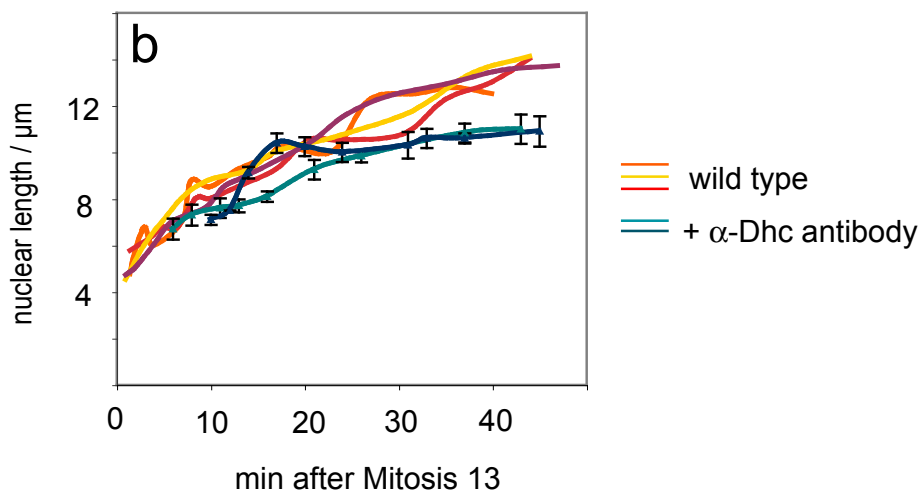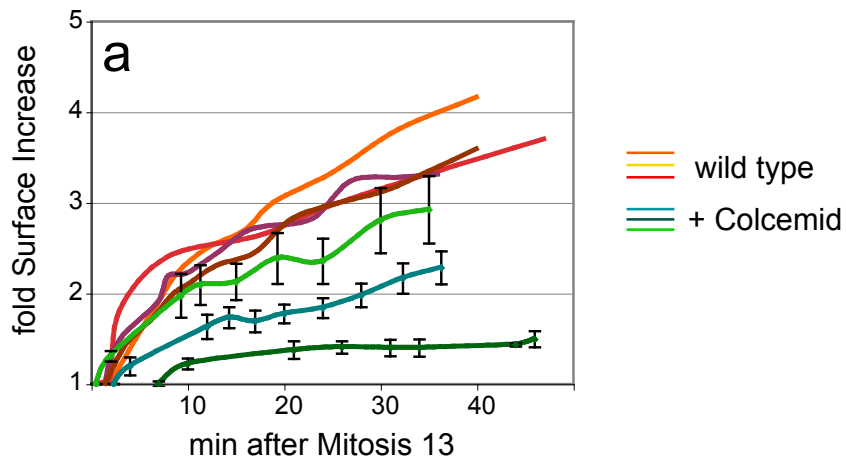H2Av::GFP residence time/ seconds

Supplementary Information Fig. S1: Nuclear Morphogenesis During *Drosophila* Cellularisation
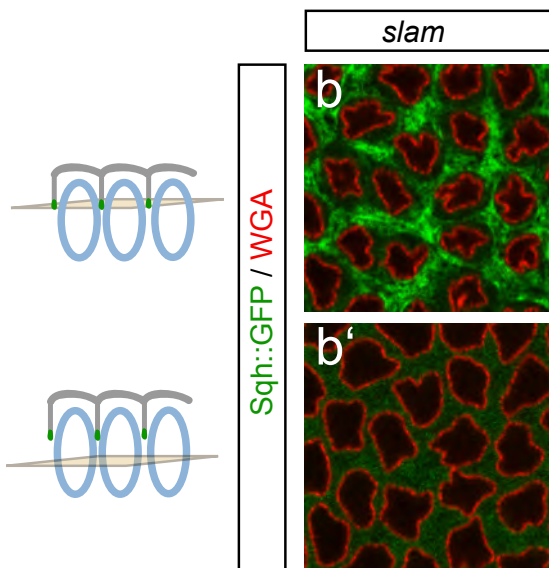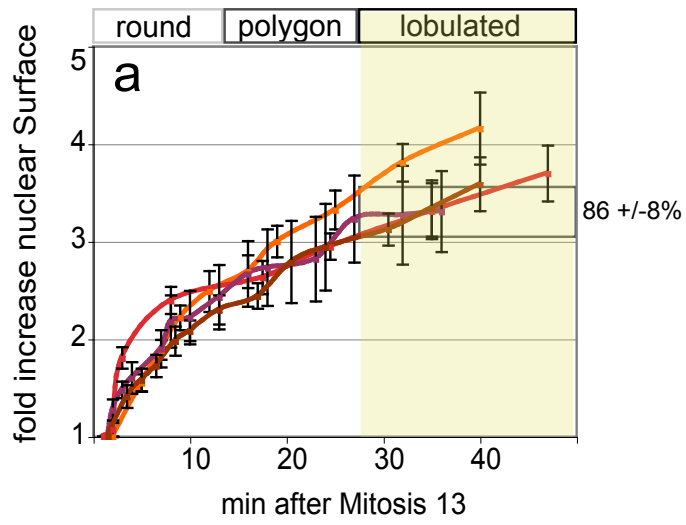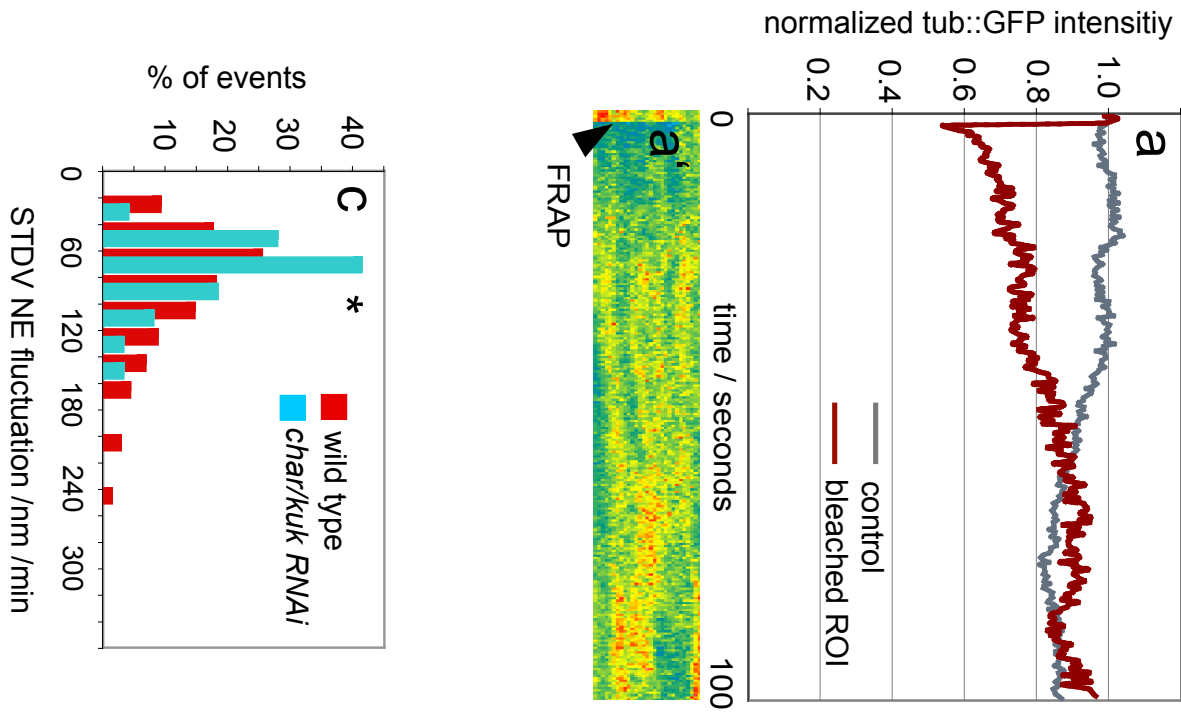
Supplementary Information Fig. S2:
Microtubules and Dynein Control Nuclear Elongation and Surface Increase

Supp Figure S3: Char/Kuk regulates NE shape independant of MTs

Supp Fig.S5: Nuclear morphogenesis contributes to Chromatin
organisation during *Drosophila* cellularisation